To be Submitted to the ApJ

The X-ray Spectral Evolution of η Carinae as Seen by *ASCA*

M. F. Corcoran[1], A. C. Fredericks[2,3], R. Petre, J. H. Swank, and S. A. Drake[1]

Laboratory for High Energy Astrophysics, Goddard Space Flight Center, Greenbelt MD 20771

ABSTRACT

Using data from the *ASCA* X-ray observatory, we examine the variations in the X-ray spectrum of the supermassive star η Carinae with an unprecedented combination of spatial and spectral resolution. We include data taken during the recent X-ray eclipse in 1997–1998, after recovery from the eclipse, and during and after an X-ray flare. We show that the eclipse variation in the X-ray spectrum is apparently confined to a decrease in the emission measure of the source. We compare our results with a simple colliding wind binary model and find that the observed spectral variations are only consistent with the binary model if there is significant high-temperature emission far from the star and/or a substantial change in the temperature distribution of the hot plasma. If contamination in the 2–10 keV band is important, the observed eclipse spectrum requires an absorbing column in excess of 10^{24} cm^{-2} for consistency with the binary model, which may indicate an increase in $\dot{M}$ from η Carinae near the time of periastron passage. The flare spectra are consistent with the variability seen in nearly simultaneous *RXTE* observations and thus confirm that η Carinae itself is the source of the flare emission. The variation in the spectrum during the flare seems confined to a change in the source emission measure. By comparing 2 observations obtained at the same phase in different X-ray cycles, we find that the current X-ray brightness of the source is slightly higher than the brightness of the source during the last cycle, perhaps indicative of a long-term increase in $\dot{M}$, not associated with the X-ray cycle.

Subject headings: η Carinae, stars: X-rays, stars: binaries

1. Introduction

η Carinae is a notorious star which exploded in 1843 or thereabouts but refuses to go away. The explosion, deemed in the literature the "Great Eruption", gave the star instant celebrity for

[1]Universities Space Research Association, 7501 Forbes Blvd, Ste 206, Seabrook, MD 20706

[2]Dept. of Astronomy, University of Maryland, College Park, MD 20742

[3]Boeing/RTS 535 Lipoa Pkwy. Ste. 200 Kihei, HI 96753

too brief a period before it faded from public view. Nearly 100 years later Gaviola (1950) showed the star to be surrounded by a peculiar nebula he called the "homunculus", which we now know to be the ejecta from this eruption. Seventeen years after that Rodgers and Searle (1967) measured an immense IR luminosity; if reprocessed photospheric radiation, this enormous brightness indicated a true stellar monster at the heart of the Galaxy's "little man". Subsequent photometric studies (Van Genderen et al. 1999; Sterken et al. 1999; Davidson 1999) from ground and from space have shown episodes of sporadic brightenings and other apparently random variability. Perhaps more telling are the periodic changes in the strength of some excited emission lines (Damineli 1996). The process driving these emission-line variations is not known precisely, though recent radical suggestions (Damineli, Conti and Lopes 1997; Corcoran et al. 1998) attribute most of the observed cyclical phenomena to interactions in a binary system. Prior to confirming any diagnosis, we need to look at the X-rays.

Descriptions of η Carinae as an X-ray source span only about 30 years. Hill et al. (1972) reported detection of an X-ray source near η Car using a large-area proportional counter flown on a Sandhawk rocket in 1970. Though neither *Copernicus* (Griffiths et al. 1974) nor the *ANS* (Mewe et al. 1976) detected any X-ray source near η Car, a source near η Car was detected by *Ariel V* (Seward et al. 1976), by *HEAO-1* (Nugent et al. 1983; Wood et al. 1984), by *Uhuru* (Forman et al. 1978), by *EXOSAT* (Warwick et al. 1988), by *OSO-8* (Becker et al. 1976; Bunner 1978) and by *GINGA* (Koyama et al. 1990). An important characteristic of these early observations is that they all utilized collimated, non-imaging detectors with differing fields of view, spectral responses and sensitivities. So from these data it was not at all clear whether η Carinae was in fact the real source of the detected X-ray emission, or if so, whether reported flux differences were a sign of actual source variability. Direct imaging by the *EINSTEIN* X-ray observatory proved that η Car was indeed a complicated X-ray source (Seward et al. 1979; Chlebowski et al. 1984), while more recently *ROSAT* (Corcoran et al. 1995) and *RXTE* observations (Ishibashi et al. 1999) have proved the variability of the X-ray flux. The *RXTE* monitoring observations have provided the most detailed study of the temporal variability ever obtained; however, the inability of *RXTE* to clearly resolve the variable emission from nearby X-ray sources compromises our understanding of the changes taking place in the X-ray spectrum, and impedes our search for physical models.

The *ASCA* X-ray observatory (Tanaka, Inoue, and Holt 1994; Serlemitsos et al. 1995) is well suited to study a crowded, variable, hot ($kT \sim$ few keV) thermal source like η Car. The *ASCA* bandpass (0.5 10 keV) covers the bulk of the observable X-ray emission from η Car; its spectral resolution enables precise determination of plasma temperatures, absorbing columns, emission measures and line strengths; and its imaging capabilities allow η Car to be easily resolved from all other strong sources in the field. Bearing in mind these advantages we undertook a focussed program of monitoring η Car with *ASCA* on a semi-annual basis, approximately one observation per observing window, starting in 1996. These observations includes 2 target of opportunity observations of η Carinae during and immediately after the occurrence of an X-ray flare detected by *RXTE*, and the only spatially resolved measurement of the high energy ($E > 3$ keV) spectrum during the X-ray

eclipse. In §2 we provide the journal of observations and discuss the data extraction. In §3 we discuss the analysis of the spectra, while in §4 we discuss the details of the X-ray spectral analysis for each observation. In §5 we offer our conclusions and discuss the impact of these data on the "binary hypothesis" and on possible flare mechanisms.

2. Observations

Though the *ASCA* observations consist of relatively few pointings, they sample most of the important intervals in the η Carinae X-ray lightcurve. Table 1 lists the *ASCA* sequence identification number and the exposure time for both the SIS0 and GIS2 detectors. We consider only data from the SIS0 and the GIS2 detectors, since these are the best calibrated detectors aboard *ASCA*. The SIS0 data are affected by degradation of the CCDs. In addition, the observations were generally obtained at different spacecraft role angles, which caused the SIS chip to sample different parts of the Carinae nebula around η Carinae. This is important, since on some of the SIS observations the X-ray source WR 25 was also detected, or other parts of the diffuse emission from the Carinae nebula were sampled, which caused differing amounts of sky background contamination on the chips and so limited our ability to ensure a consistent correction for local sky background by direct subtraction of source free regions of the SIS chip. Using a consistent background correction is important in order that reliable changes in the spectral parameters (kT, N_H, and emission measure) can be measured. In this regard the GIS data have the advantage, since the GIS samples a roughly 1 degree region around η Carinae, making it is possible to use a consistent region for correction of sky background for all the GIS observations, regardless of spacecraft roll angle.

Following the data extraction methods used previously (Corcoran et al. 1998), we derived good X-ray events from the unfiltered processed *ASCA* data by excluding times of SAA passage and intervals when the earth elevation angle was less than 5° for the GIS data and less than 10° (20° for bright earth) for the SIS data. We also excluded times of low geomagnetic rigidity, and times when the satellite pointing was more than 0.01° from the nominal position of η Carinae. SIS data were cleaned of events caused by "hot" and "flickering" CCD pixels, and the GIS data were cleaned of calibration source events and other background events based on rise-time discrimination.

We extracted images from the screened events using the XSELECT analysis software provided and maintained by the High Energy Astrophysics Science Archive Research Center at the Goddard Space Flight Center. As the spatial resolution of *ASCA* is only about 1 arcminute, the extracted spectra from η Carinae will include emission from very nearby sources, in particular diffuse sky photons and the O3 star HDE 303308. *ROSAT* data show that the diffuse emission near η Carinae and HDE 303308 are fairly soft (typically $kT < 0.5$ keV), so that this contamination should not have much effect on the shape of the spectrum of η Carinae at energies above 2 keV; but these sources will have significant influence on the softest emission below 1 keV.

For the GIS data analysis, we defined source and background regions directly on the GIS image

for each observation. We chose circular source regions centered on η Carinae of radius $\approx 3'$ (large enough to include almost all the flux from η Carinae but small enough to exclude contaminating photons from the nearby X-ray source WR 25). We used background regions with the same radius as the source region, centered at approximately the same apparently source-free location in the Carina nebula relative to η Carinae to reduce the chance of spurious variability. We extracted source and background spectra using the XSELECT software, and before analysis the source spectra were rebinned so that there were a minimum of 10 counts per channel. Prior to fitting the spectra (using the XSPEC analysis package) we created appropriate effective area corrections for each observation to account for variations in the placement of the source on the detector.

3. Model Fitting

We modelled the SIS0 and GIS2 spectra of η Carinae using a template based on the best fit model published in Corcoran et al. (1998). That model included a variable abundance soft thermal component (the "vmekal" model in XSPEC terminology) at a temperature near 0.5 keV, and a hard, absorbed thermal component with a temperature near 5 keV. We also assumed the abundances derived in Corcoran et al. (1998) for our modeling. In general this will not have much influence on our modeling of the high-energy spectrum, since the strong lines observable in the hot component all have near-solar abundances. The soft thermal component is primarily produced by an elliptical ring of emission at a distance of about $15''$ from the star, and thus should not vary. The hard component is thought to be dominated by the emission originating within $0.5''$ of the star, and is variable (Corcoran et al. 1995; Ishibashi et al. 1999). Therefore we first fit the data by allowing the spectral parameters (kT, N_H and emission measure) of the 5-keV source to vary, keeping the spectral parameters of the soft component fixed. Generally this resulted in adequate fits to the GIS2 spectra, but not the SIS0 spectra. The variations in the soft part of the SIS spectra are probably a reflection of the degradation of the soft response of the SIS detectors and/or contamination by WR 25, rather than any real change in the soft emission of around η Carinae. Since the soft and hard components are not well resolved by *ASCA*, any uncertainty in modeling the soft component will influence the derived spectral parameters (especially N_H) for the hard component. Due to these apparently instrumental effects in the SIS data, in the following we concentrate our analysis on the GIS data.

The model parameters (kT, N_H, the emission measure EM and the equivalent width of the fluorescent Fe K line EW_{Fe}, along with the observed luminosity and the unabsorbed luminosity in the 2–10 keV band) we derived by fitting the GIS2 data are given in table 1. The error bars quoted in the table are 90% formal confidence intervals for the parameters. Since we are mainly interested in relative variations in the parameters, we have not attempted to include systematic uncertainties (as would arise, for example, if our assumed spectral model was incorrect, or if the sky correction was not a good approximation to the cosmic background at the position of η Carinae). The "deconvolved" spectra are shown in figure 1. The data are represented by error bars while

the solid lines show the soft and hard thermal components. These components cross at an energy near 1.5 keV, which means that the emission below 1.5 keV is dominated by the soft component, and the emission above 1.5 keV is dominated by the hard component. The amount of absorption appropriate to the hard component is determined mainly by the magnitude of the cutoff in the hard emission near 1.5 keV. Figure 2 highlights the Fe-K line region in each of the six spectra. The variations in the derived spectral parameters as a function of time are shown in figures 3 and 4.

4. Discussion

4.1. The Eclipse Spectrum and the Binary Star Model

The *ASCA* spectrum obtained on Dec 24 1997 at the start of the X-ray eclipse provides fairly stringent constraints on the mechanism responsible for the 2–10 keV emission, and in principle provides the best available test of the colliding wind binary model. This spectrum shows that the change in X-ray flux during the eclipse is apparently due to a drop in the emission measure of the hard source, and that neither the observed column to the source (as measured by the turnover in the hard emission component near 1.5 keV), the temperature of the source (as measured by the distribution of emission above 1.5 keV), nor the continuum flux above 5 keV show any measurable increase at this time. According to models of colliding wind emission (Usov 1992), the intrinsic luminosity from the colliding wind shock is proportional to the inverse of the stellar separation. Thus the intrinsic luminosity of the colliding wind source should have been near its maximum at this time, since this observation should have been closest to periastron passage (Damineli, Conti and Lopes 1997). However, since the line of sight to the colliding wind source passes through the wind from η Carinae at this time, the observed emission should be significantly attenuated by η Carinae's wind. To test the colliding wind model, we tried to fit the eclipse spectrum by increasing the flux of and the absorption to the hard component to produce an overall reduction in the observed X-ray spectrum. Following Usov (1992), near the time of the *ASCA* low-state observation, the intrinsic 2-10 keV X-ray luminosity should have been $L_x \sim 7 \times 10^{35}$ ergs s^{-1} (assuming a distance to η Carinae of 2600 pc and an eccentricity $e \approx 0.8$ and the stellar and wind parameters given in Ishibashi et al. 1999), or about a factor of 8.5 larger than the intrinsic luminosity far from periastron. We then fixed the intrinsic luminosity of the hard component at 7×10^{35} ergs s^{-1}, and tried to reproduce the observed eclipse spectrum by increasing the absorbing column to the hard source. As illustrated in figure 5, attempts to model the *ASCA* eclipse spectrum by varying the absorbing column alone underpredict the observed emission near 2 keV. Thus, if there are no other sources of 2–10 keV emission within the *ASCA* source extraction region, the observed eclipse spectrum is inconsistent with simple colliding wind models in which the source flux varies as $1/D$ with no change in intrinsic spectral shape.

Another effect which could in principle produce the eclipse spectrum measured by *ASCA* could be a decrease in the temperature of the colliding wind source, either produced by radiative braking

(Gayley, Owocki, and Cranmer 1997) or strong cooling of the wind near periastron, or if the winds collide at periastron at speeds which are much lower than the wind terminal velocities. To explore the effects of a decrease in temperature of the colliding wind source, we attempted to model the observed eclipse spectrum by assuming that the temperature in the wind-wind collision shock is only 0.5 keV at periastron. As seen in figure 5, this "cool source" model can provided an adequate description of the emission near 2 keV in the eclipse spectrum but underpredicts the amount of emission at energies above 5 keV. It is possible that a distributed emission model, consisting of hard, heavily absorbed emission plus softer emission at a lower column could perhaps be devised so as to fit the observed *ASCA* eclipse spectrum. However, there is no evidence in any of the other *ASCA* η Carinae spectra for any such complicated distribution of emission.

A third possibility is that the wind from η Carinae is so thick that none of the colliding wind emission is seen by *ASCA*. In this case the 2–10 keV emission during the eclipse would necessarily be contamination by another source somewhere within the 3′ *ASCA* extraction region, and thus not characteristic of the colliding wind source. To further explore this possibility, we assume that the colliding wind source is completely hidden at the time of the *ASCA* eclipse spectrum, and that all of the 2–10 keV flux seen in the *ASCA* eclipse spectrum is contamination from a faint source located somewhere beyond the stellar source. We can then use the expected increase in intrinsic L_x at the 1998.0 periastron passage to provide an estimate of the amount of absorption needed to completely hide the colliding wind source in the 2–10 keV band. If the intrinsic 2–10 keV L_x was 7×10^{35} ergs s^{-1} near the time of the *ASCA* eclipse observation as expected from the colliding wind model, then the total column to the X-ray source would need to be $N_H > 3 \times 10^{24}$ cm^{-2} in order to completely hide this much luminosity. If the wind from η Carinae provides all the absorbing material, and if the wind is spherically symmetric, then the mass loss rate from η Carinae near periastron would need to be $\dot{M} > 10^{-2} M_\odot$ yr^{-1} if $V_\infty = 500$ km s^{-1} and the periastron separation is 3 AU (Damineli, Conti and Lopes 1997). This is more than a factor of 10 larger than the generally accepted value of the mass loss from η Carinae (Davidson 1999). A value of $\dot{M} > 10^{-2} M_\odot$ yr^{-1} could not be characteristic of the mass loss rate of the star at other orbital phases away from periastron, since if it were then the expected X-ray luminosity would be about a factor of 10 larger than the observed L_x at phases outside periastron. Thus, in the context of the binary model, the *ASCA* eclipse spectrum may raise the interesting possibility of a significant increase in $\dot{M}$ near periastron, if the wind from η Carinae provides all the absorption to the X-ray source. However, if the stellar photosphere or other wind structures (like the "wind-disk" considered by Ishibashi et al. 1999) provides significant obscuration of the X-ray source, then the *ASCA* low-state spectrum could be matched by a much smaller wind mass loss rate.

4.2. The Fe K fluorescent line

The Fe K fluorescent line is produced by scattering of photons from the stellar source, and so in theory offers another diagnostic about the conditions of the X-ray region associated with

the star. As noted in Corcoran et al. (1998), the equivalent width of the Fe K fluorescent line is in general related to the column density of scatterers by $EW \approx 2.3 N_{24}$ keV, where EW is the equivalent width of the line in keV and N_{24} the total column density of cold material in units of 10^{24} cm^{-2} (Kallman 1995). Taking the ratio of the Fe line equivalent widths to the column densities of the hard component, the *ASCA* spectra suggest that $EW \approx 4 - 7 N_{24}$ for η Carinae outside of eclipse. As seen in Table 1, during the eclipse the equivalent width of the Fe K fluorescent line is about a factor of 2–5 larger than at any other time, suggestive of a maximum in number of scatterers along the line of site at this time. From Table 1, $EW \sim 0.5 - 0.8$ keV, which suggests that $N_H > 10^{24}$ cm^{-2}. A column so large is consistent with complete absorption of the hard source. This provides some support for either an increase in mass loss rate near periastron, or the presence of an additional absorber in the line of sight at the time of periastron. However, since the Fe fluorescent line is not fully resolved from the thermal line by *ASCA*, we regard the line analysis as supportive of an absorption enhancement in December 1997 but not necessarily conclusive proof of such an enhancement at that time.

4.3. The Flare and Post-Flare Spectrum

One of the first and most surprising discoveries of the *RXTE* monitoring of η Carinae was the discovery of short-term (days-weeks) variations in the X-ray emission which appeared periodic (Ishibashi et al. 1997; Corcoran et al. 1997; Ishibashi et al. 1999). The origin of these "flares" was and is still uncertain; since the PCA offers no spatial resolution, there remained the real possibility that the flares originated in another serendipitous source in the PCA field of view.

Based on the *RXTE* lightcurve flare ephemeris two *ASCA* target of opportunity observations were scheduled, the first near X-ray flare maximum, the second about 2 weeks after the flare maximum. These *ASCA* observations clearly showed that the X-ray flux changed in a manner consistent with coincident *RXTE* measures, confirmin η Carinae as the flaring source. Our analysis of the spectra indicates that the flare phenomena is dominated by a change in emission measure, with no measurable change in either source temperature or column density. This suggests a mechanism in which the only change in the X-ray emitting zone is an increase in density during the flare. This is consistent with models (Corcoran et al. 1997; Davidson, Ishibashi and Corcoran 1998) in which the flares are produced by periodic ejections of shells of matter from the primary star, which then provide an increase in density in the X-ray zone at some location far from the star. These models suggest that the flare period represents either a pulsation period of the star, or a rotation period if the wind is azimuthally anisotropic. The existence of flaring by itself does not require the presence of a binary companion, but as noted in Ishibashi et al. (1999), the variations in the period of the flares following the eclipse are consistent with the presence of a companion.

4.4. The $\phi = 0.2$ Spectra

Our *ASCA* observation 27023000 (February 1999) and the very first *ASCA* observation of η Carinae in August 1993 (Tsuboi et al. 1997) were both obtained at $\phi = 0.2$ according to the ephemeris of Damineli, Conti and Lopes (1997). Comparison of these spectra provides important information about the cycle-to-cycle repeatability of the X-ray emission. We extracted the archived August 1993 GIS2 spectrum and compared the 2 spectra. We found that that the observed 2–10-keV X-ray luminosity in 1993 was $4.7 \pm 0.1 \times 10^{34}$ erg s^{-1}, while the observed X-ray luminosity in February 1999 was about $5.1 \pm 0.2 \times 10^{34}$ erg s^{-1}, an increase of 8.5%. This suggests some modest amount of non-phase-locked variability in the X-ray emission. The brightening seen in the 1999 data could result if these data were obtained during an X-ray flare, but the *RXTE* 2–10 keV X-ray flux for $\pm$20 days around the latter *ASCA* observation (1999 January 20 – March 1) shows no evidence of any flare activity (in fact the *RXTE* data suggest a steady decline in the X-ray flux during this interval). Thus the observed brightening in the *ASCA* spectra suggests that an overall brightening of the 2–10 keV X-ray flux has occurred, and that this brightening is not directly tied to the Damineli, Conti and Lopes (1997) cycle. The X-ray brightening may be related to a long-term increase in the optical brightness of the star (Van Genderen et al. 1999) and/or the recent brightening at UV, optical and infrared wavelengths (Sterken et al. 1999; Davidson et al. 1999). While the optical, IR and UV brightening could be produced in part by a decrease in extinction produced by material in the homunculus, the X-ray brightening we report is probably not the result of a decrease in circumstellar absorption, since at the (relatively) low column density through the homunculus ($N_H \approx 10^{21}$ cm^{-2}), circumstellar absorption is negligible at energies above 2 keV. Our analysis suggests that the flux increase is primarily due to an increase in the emission measure of the X-ray emitting region during the interval 1993-1999. Since the emission measure is related to the mass loss rate, this implies an increase in $\dot{M}$ in the 1993–1999 interval which is not tied to the X-ray cycle.

5. Conclusions

In this paper we present analysis of *ASCA* spectra of the extremely luminous star η Carinae. These spectra provide the best description of the X-ray emission of the star yet obtained, and sample all the important states of the star's X-ray variability. While we confirm the fundamental variability of the X-ray emission as first noted by Corcoran et al. (1995) and later in the more detailed study of Ishibashi et al. (1999), probably the most important result of this *ASCA* monitoring is that we detect no direct increase in the column density to the hot source in any of the observed spectra, but especially in the spectra obtained during the eclipse in 1997.9, and that the 1997.9 spectrum does not show any increase in emission out to energies of 10 keV. This could be interpreted as evidence that the binary model is incorrect; however, we feel that a more likely explanation is that the *ASCA* spectra are contaminated by hard emission ($kT \sim 2$ keV) relatively far from the star (but within or near the homunculus). Contamination however also implies that either the

wind from η Carinae is significantly non-spherical, or that there is a substantial increase in $\dot{M}$ from η Carinae near periastron. Interestingly the value of N_H implied by the equivalent width of the Fe K line fluorescent line provides indirect evidence of an increase in the absorbing column to the hot source. Finally, our analysis of the flare spectra suggests that the flare mechanism could be produced by periodic ejection of a shell of material (presumably due to an underlying stellar pulsation), and the interaction of this shell with an X-ray emitting region near the star. The *ASCA* data are generally consistent with the notion that η Carinae is a binary system in which the primary pulsates with $P \sim 85$ days and in which the orbital period is about 5.52 years, but these data also suggest that interactions between the stellar components may be more important than one would initially assume. The *ASCA* data also suggest that the wind from the primary is structured (or that mass loss is non-isotropic from the stellar surface) and/or that the mass loss rate is not constant, and may experience a significant increase when the system is enters the eclipse (coincidentally near periastron passage). Higher spatial and spectral resolution observations of the kind obtainable with *CHANDRA* and *XMM*, especially during the low state, will be extremely valuable for determining the level of hard X-ray contamination and for clarifying many of the issues raised by the *ASCA* spectra.

We would like to thank the *ASCA* staffs at ISAS and GSFC for the extra effort they made in scheduling these observations, especially the granting of TOO time to observe the two flare spectra, and in re-scheduling the eclipse observation at the start of the eclipse. In particular we'd like to thank F. Nagase, R. Fujimoto, P. Hilton, I. Yamagishi, M. Ishida, E. Pier, K. Mukai, and N. White. This work was supported by NASA grant NAS5-32490: this support is most gratefully appreciated. We made use of the FTOOLS suite of software supported by the HEASARC, and of the *ASCA* data archives also maintained at the HEASARC. This research has made use of NASA's Astrophysics Data System Abstract Service.

REFERENCES

Becker et al., 1976, ApJ, 209, L65

Bunner, A., 1978, ApJ, 220, 261

Chlebowski, T., et al., 1984, ApJ, 281, 665

Corcoran, M. F., et al., 1995, ApJ, 445, L121

Corcoran, M. F., et al., 1997, Nature, 390, 587

Corcoran, M. F., et al., 1998, ApJ, 494, 381

Damineli, A., 1996, ApJ, 460, L49

Damineli, A., Conti, P. S., Lopes, D. F., 1997, New Astronomy, 2, 107

Davidson, K., ASP Conf Ser., 179, 6

Davidson, K., Ishibashi, K., and Corcoran, M. F., 1998, New A., 3, 241

Davidson, K., et al., 1986, ApJ, 305, 867

Davidson, K., et al., 1999, AJ, 118, 1777

Davidson, K., Walborn, N. R., and Gull, T. R., 1982, ApJ254, L47

Duncan,R.A., et al., 1995, ApJ, 441, L73

Forman, W., et al., 1978, ApJS, 357, 412

Gaviola, E., 1950, ApJ, 111, 408

Gayley, K., Owocki, S. P., and Cranmer, S., 1997, ApJ, 474, 786

Griffiths, R. E., et al., 1974, Nature, 250, 714

Hill et al., 1972, ApJ, 171, 519

Ishibashi, K., et al., 1997, IAU Circ., 6668

Ishibashi, K., et al., 1999, ApJ, 524, 983

Kallman, T., 1995, ApJ, 455, 603

Koyama,K., et al., 1990, ApJ, 362, 215

Mewe, R., et al., 1976, Ap&SS, 42, 217

Nugent, J. J., et al., 1983, ApJS, 51, 1

Pittard, J. M., et al., 1998, MNRAS, 299, L5

Rodgers, A. W., and Searle, L., 1967, MNRAS, 135, 99

Serlemitsos, P., et al., 1995, PASJ, 48, 171

Seward, F. D., and Chlebowski, T. 1982, ApJ, 256, 530

Seward, F., et al., 1976, MNRAS,177, 13P

Seward, F., et al., 1979, ApJ, 234, L55.

Sterken, C., Freyhammer, L., Arentoft, T., and van Genderen, A. M., 1999, A&A, 346, 33

Stevens, I. R., Blondin, J. M., and Pollock, A. M. T., 1992, ApJ, 386, 265

Tanaka, Y., Inoue, H., Holt, S. S., 1994, PASJ, 46, L37

Tsuboi, Y., et al., 1997, PASJ, 49, 85

Usov, V. V., 1992, ApJ, 389, 635

van Genderen, A. M., Sterken, C., de Groot, M., and Burki, G., 1999, A&A, 343, 847

Viotti, R., et al., 1999, ASP Conf Ser., 179, 275

Warwick, R. S., et al., 1988, MNRAS, 232, 551

Wood, K. S., et al., 1984, ApJS, 56, 507

Fig. 1.— X-ray spectra of η Carinae from the *ASCA* GIS2 detector. a) TOO observation of July 3 1997 (dataset 110504000) obtained during an X-ray flare; b) TOO observation of July 19 1997 (dataset 11504010); c) observation of December 24 1997 (dataset 26033000) obtained at the start of the eclipse; d) observation of July 16 1998 (dataset 26034000), first *ASCA* observation after the end of the eclipse; e) observation of February 8 1999 (dataset 27023000) obtained near a STIS observation; and f) observation of June 14 1999 (dataset 27024000). The cool and hot components and the fluorescent Fe line are shown by thin histograms, the data by crosses. The most dramatic change in the spectrum occurred during the eclipse, while variability in the spectra outside of eclipse is more subtle.

Fig. 2.— X-ray spectra of η Carinae from the *ASCA* GIS2 detector emphasizing the Fe K-line region. a) TOO observation of July 3 1997 (dataset 110504000) obtained during an X-ray flare; b) TOO observation of July 19 1997 (dataset 11504010); c) observation of December 24 1997 (dataset 26033000) obtained at the start of the eclipse; d) observation of July 16 1998 (dataset 26034000), first *ASCA* observation after the end of the "low state"; e) observation of February 8 1999 (dataset 27023000) obtained near a STIS observation; and f) observation of June 14 1999 (dataset 27024000). Fluorescent Fe K emission is shown by the thick line near 6.4 keV, while the feature near 6.7 keV is a thermal line present in the assumed model. Note that the fluorescent line is always weaker than the thermal line except for the eclipse observation, at which time the line strengths are reversed.

Fig. 3. Variation of the column density N_H to the hard source, along with the variation in the equivalent width of the Fe K fluorescent line. The increase in the equivalent width of the Fe line at the time of the X-ray eclipse (JD 2,450,808.04) suggests an extraordinarily large amount of absorption to the hard source; this can only be reconciled with the drop in N_H from direct continuum fitting if the continuum is contaminated by hard emission from a source beyond the star, though within the *ASCA* extraction region.

Fig. 4. Variation of kT and L_x of the hard source. No real change is seen in kT, while both the observed and absorption-corrected ("intrinsic") luminosity show minima during the X-ray eclipse.

Fig. 5. Comparison of the observed eclipse spectra and simple colliding wind models a) in which the luminosity of the colliding wind source is fixed at $L_x = 7 \times 10^{35}$ ergs s^{-1}, and the absorption to the colliding wind source allowed to increase (dashed line), and b) in which the temperature of the colliding wind source is assumed to be 0.5 keV, with the emission measure of and the column to the colliding wind source allowed to vary (dotted line). Neither model alone adequately fits the observed eclipse spectrum. The best fit to the eclipse spectrum given in Table 1 is shown by the solid line.

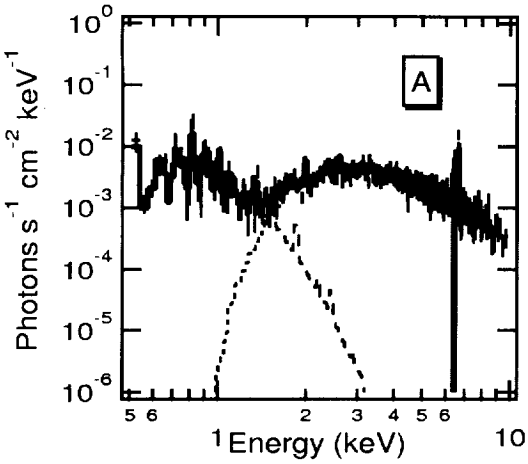
A
Photons s^{-1} cm^{-2} keV^{-1}
10^{0}
10^{-1}
10^{-2}
10^{-3}
10^{-4}
10^{-5}
10^{-6}
5 6
2 3 4 5 6
1
10
Energy (keV)

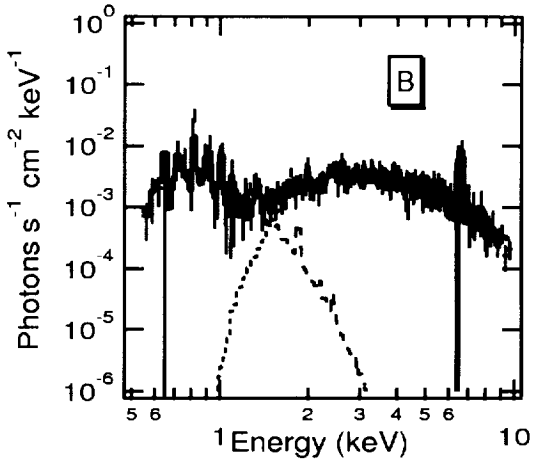
B
Photons s^{-1} cm^{-2} keV^{-1}
10^{0}
10^{-1}
10^{-2}
10^{-3}
10^{-4}
10^{-5}
10^{-6}
5 6
2 3 4 5 6
1
10
Energy (keV)

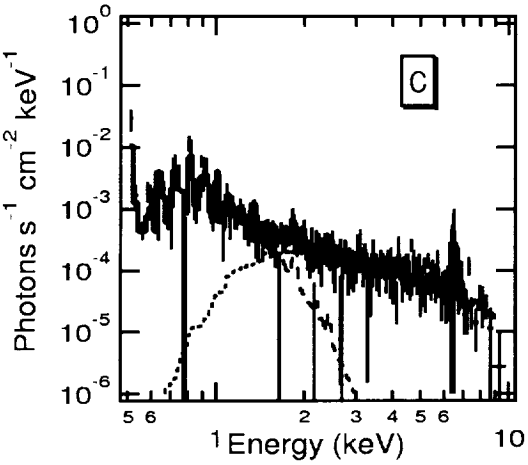
C
Photons s^{-1} cm^{-2} keV^{-1}
10^{0}
10^{-1}
10^{-2}
10^{-3}
10^{-4}
10^{-5}
10^{-6}
5 6
2 3 4 5 6
1
10
Energy (keV)

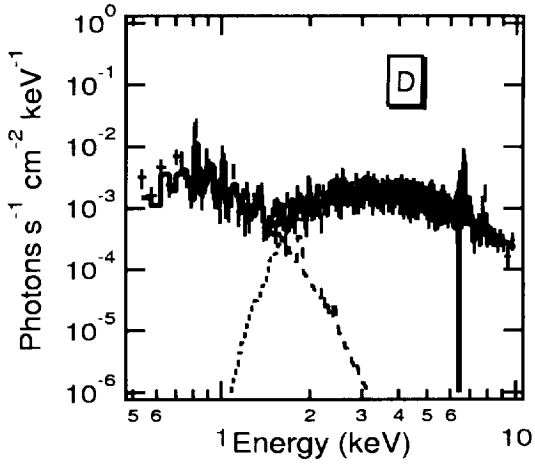
D
Photons s^{-1} cm^{-2} keV^{-1}
10^{0}
10^{-1}
10^{-2}
10^{-3}
10^{-4}
10^{-5}
10^{-6}
5 6
2 3 4 5 6
1
10
Energy (keV)

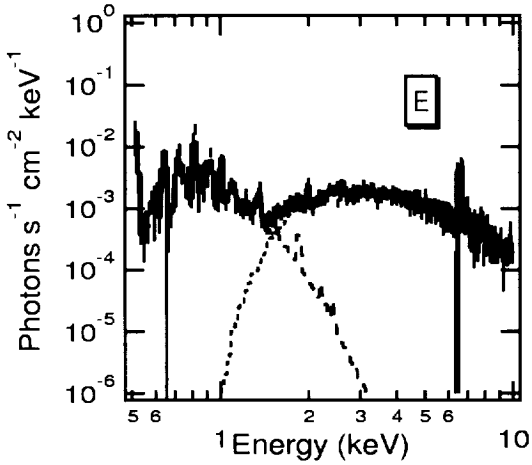
E
Photons s^{-1} cm^{-2} keV^{-1}
10^{0}
10^{-1}
10^{-2}
10^{-3}
10^{-4}
10^{-5}
10^{-6}
5 6
2 3 4 5 6
1
10
Energy (keV)

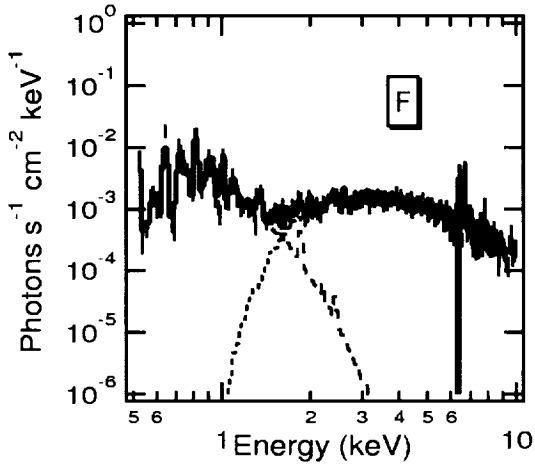
F
Photons s^{-1} cm^{-2} keV^{-1}
10^{0}
10^{-1}
10^{-2}
10^{-3}
10^{-4}
10^{-5}
10^{-6}
5 6
2 3 4 5 6
1
10
Energy (keV)

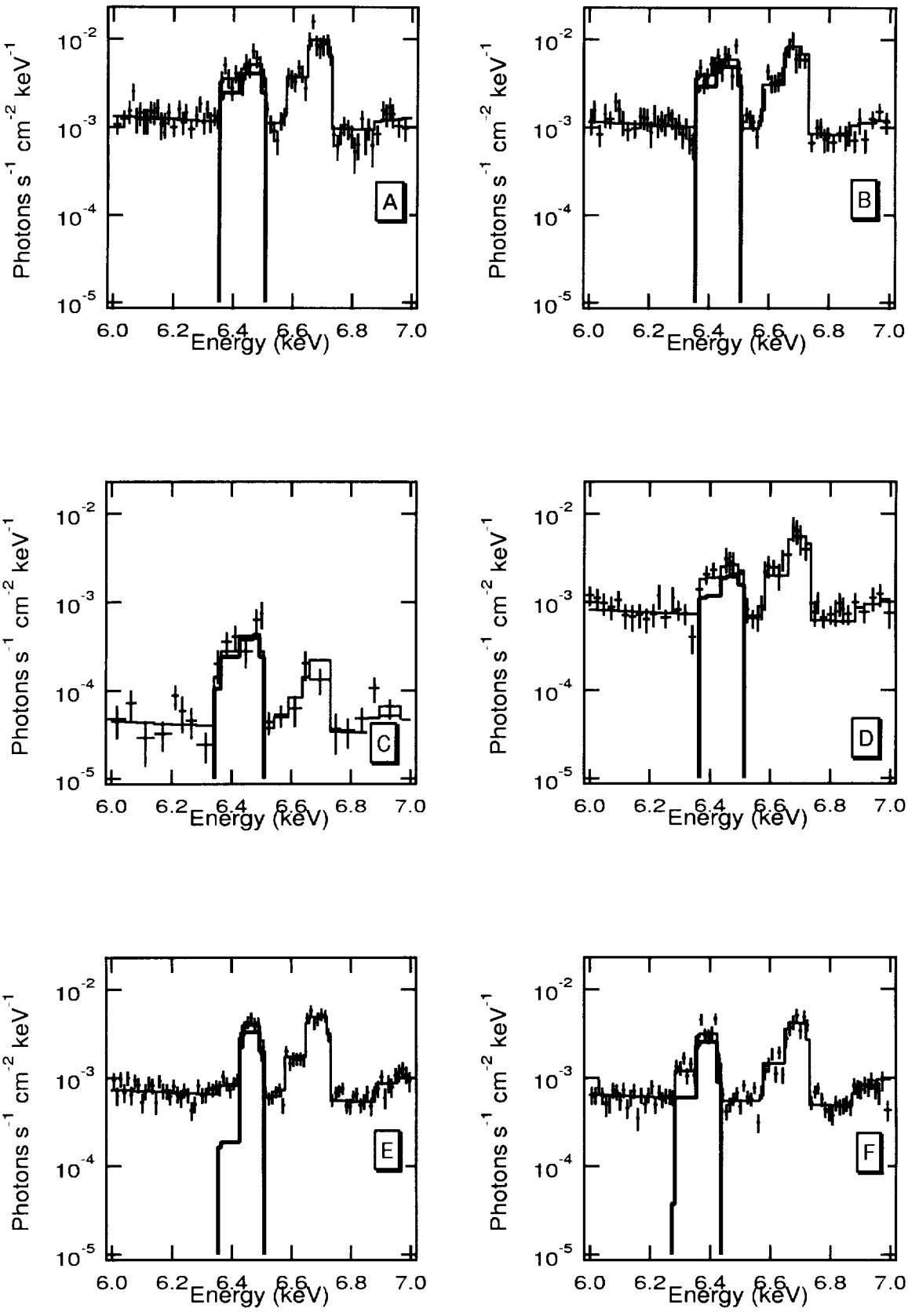
Photons s^{-1} cm^{-2} keV^{-1}
10^{-2}
10^{-3}
10^{-4}
10^{-5}
6.0
6.2
6.4
6.6
6.8
7.0
Energy (keV)
A
B
C
D
E
F

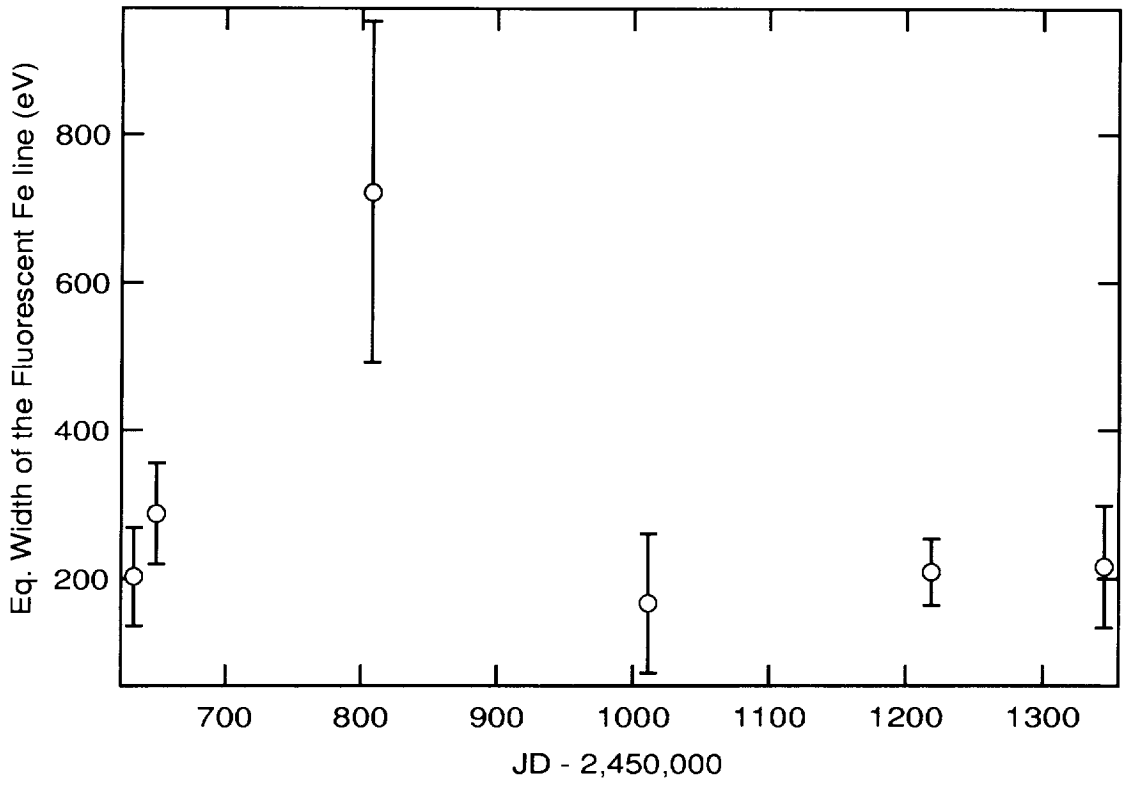
Eq. Width of the Fluorescent Fe line (eV)
800
600
400
200
700
800
900
1000
1100
1200
1300
JD - 2,450,000

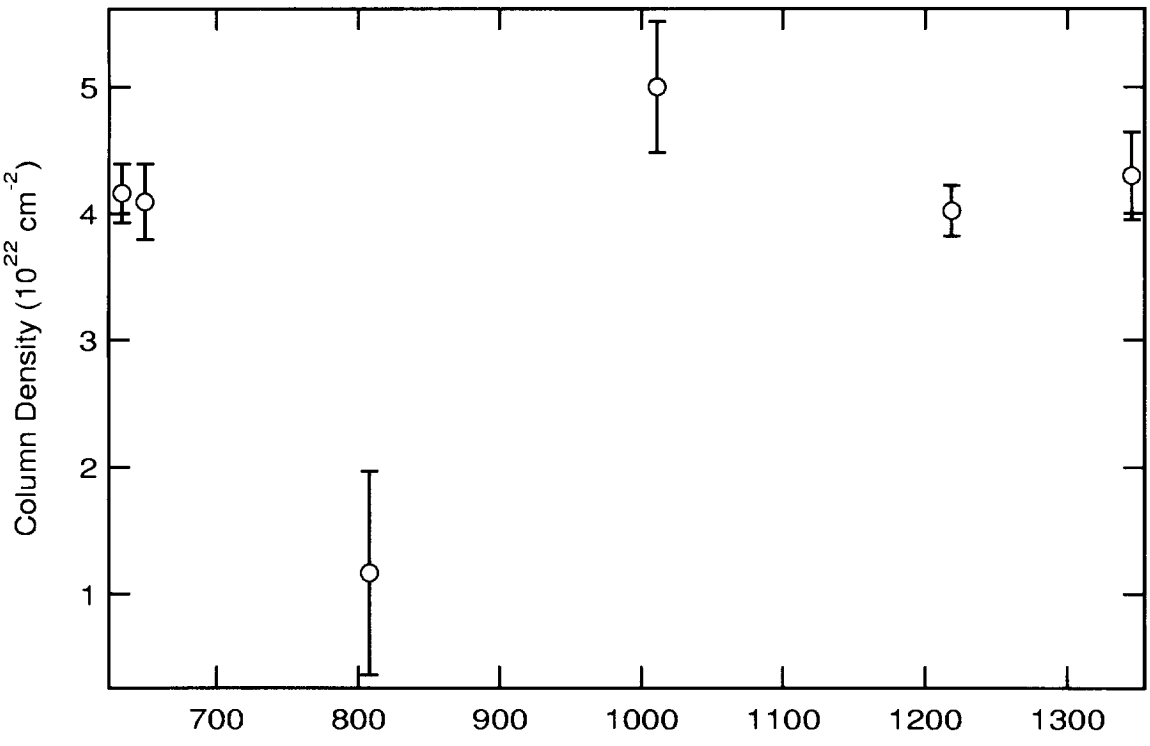
Column Density (10^{22} cm^{-2})
5
4
3
2
1
700
800
900
1000
1100
1200
1300

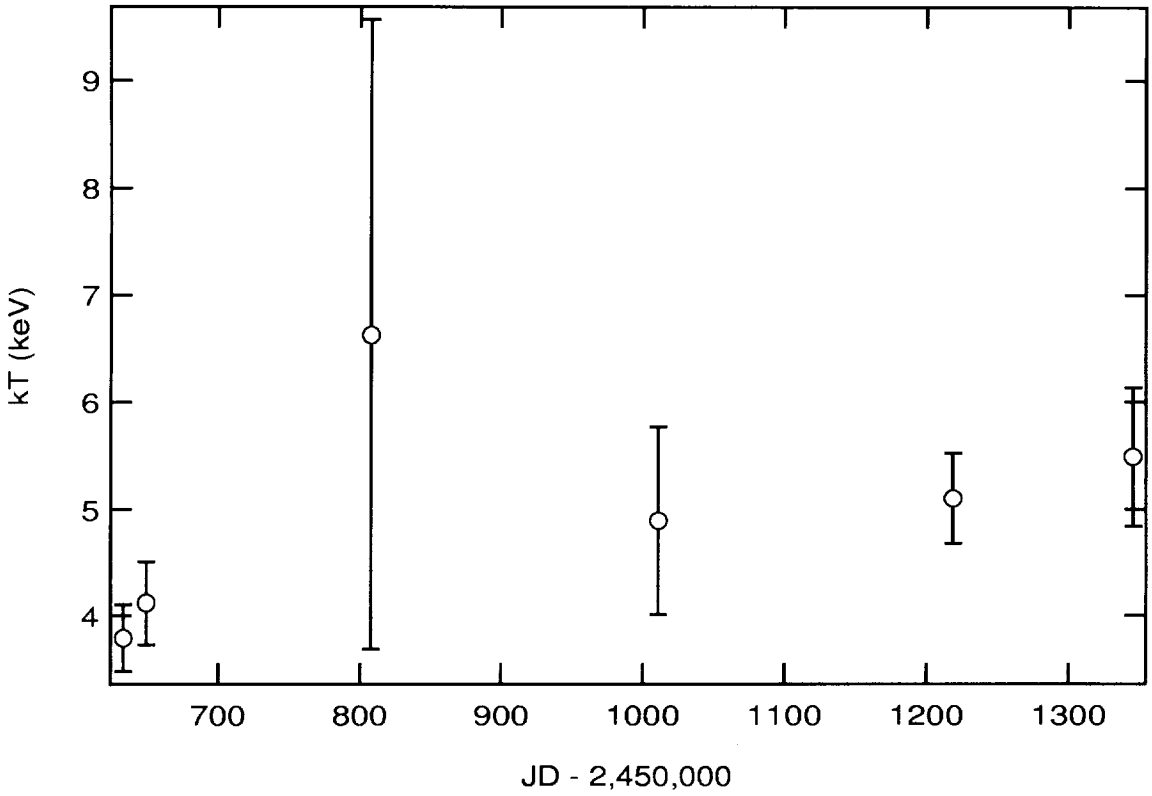
kT (keV)
9
8
7
6
5
4
700
800
900
1000
1100
1200
1300
JD - 2,450,000

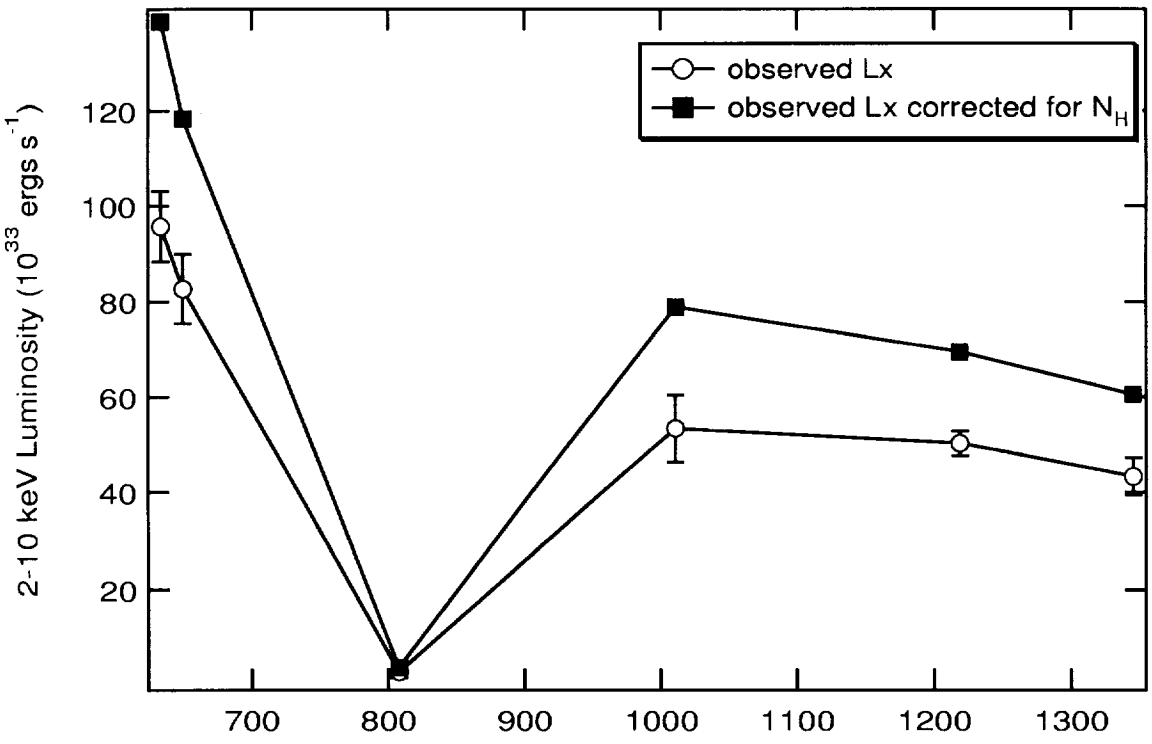
observed Lx
observed Lx corrected for N_H
2-10 keV Luminosity (10^{33} ergs s^{-1})
120
100
80
60
40
20
700
800
900
1000
1100
1200
1300

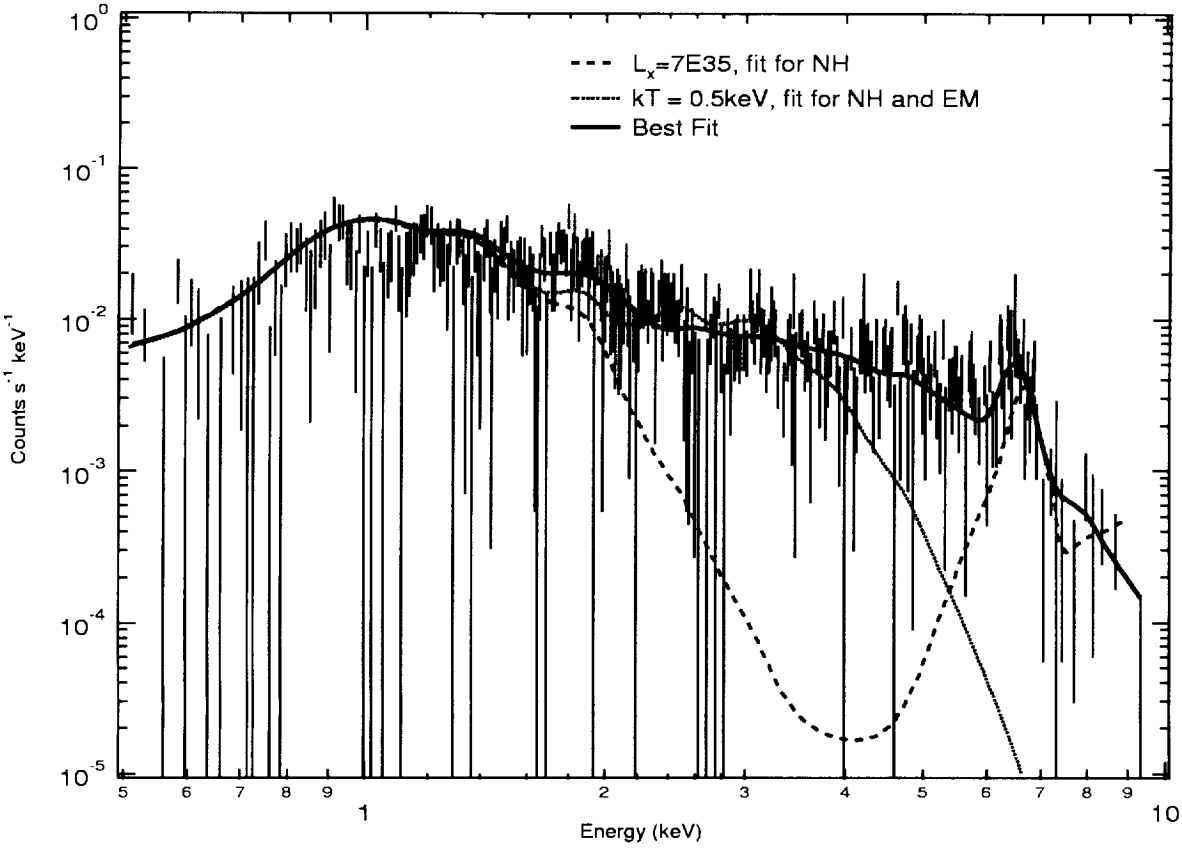
L_x=7E35, fit for NH
kT = 0.5keV, fit for NH and EM
Best Fit
Counts s^{-1} keV^{-1}
Energy (keV)

		11504000 Jul 3 1997		11504010 Jul 19 1997	
Parameter	Units	SIS0	GIS2	SIS0	GIS2
Date[1]	TJD[2]	633.18 ± 0.27	633.18 ± 0.27	649.40 ± 0.27	649.40 ± 0.27
Exposure	s	1.5449E+04	1.2620E+04	8496	1.2768E+04
$N_{H,2}^3$	10^{22} cm^{-2}	4.09±0.16	4.16±0.23	4.31±0.34	4.09±0.30
T_2	keV	4.77±0.40	3.79±0.31	5.23±0.92	4.12±0.39
EM_2	10^{57} cm^{-3}	9.89±0.57	12.09±0.89	8.63±0.90	9.60±0.89
EW_{Fe}	eV	76.6	203.0±66.0	135.0±76.8	288.0±68.0
EM_1	10^{57} cm^{-3}	1.20	1.90±0.30	1.24±0.11	1.66±0.20
χ^2_ν		1.10	0.91	0.74	1.09
L_x	10^{33} ergs s^{-1}	90.81±4.86	95.70±7.32	76.61±8.92	82.72±7.30
$L_{x,unab}$	10^{33} ergs s^{-1}	128.99	138.68	120.03	118.41

		26033000 Dec 24 1997		26034000 Jul 16 1998	
Parameter	Units	SIS0	GIS2	SIS0	GIS2
Date	TJD	808.04 ± 0.65	808.05 ± 0.63	1011.06 ± 0.37	1011.06 ± 0.37
Exposure	s	3.0769E+04	5.8591E+04	9269	1.3351E+04
$N_{H,2}$	10^{22} cm^{-2}	2.67±1.65	1.17±0.80	4.80±0.40	5.00±0.52
kT_2	keV	10.0±5.1	6.63±2.94	6.56±1.51	4.89±0.88
EM_2	10^{57} cm^{-3}	0.195±0.084	0.240±0.085	5.17±0.54	5.90±0.84
EW_{Fe}	eV	806.0±693.0	721.0±230.0	162.0±87.6	167.0±93.6
EM_1	10^{57} cm^{-3}	0.692±0.066	0.827±0.124	1.20±0.12	1.27±0.24
χ^2_ν		1.04	1.17	1.02	0.92
L_x	10^{33} ergs s^{-1}	3.03±1.14	3.62±0.88	55.92±5.67	53.36±7.05
$L_{x,unab}$	10^{33} ergs s^{-1}	3.67	4.03	79.40	78.91

		27023000 Feb 8 1999		27024000 Jun 14 1999	
Parameter	Units	SIS0	GIS2	SIS0	GIS0
Date	TJD	1218.74 ± 0.68	1218.75 ± 0.68	1345.00 ± 0.92	1345.00 ± 0.92
Exposure	s	3.8676E+04	5.3746E+04	3.7949E+04	5.1843E+04
$N_{H,2}$	10^{22} cm^{-2}	3.97±0.21	4.02±0.20	3.97±0.22	4.30±0.35
kT_2	keV	6.59±0.81	5.10±0.42	8.61±1.69	5.49±0.65
EM_2	10^{57} cm^{-3}	4.50±0.24	5.04±0.28	3.63±0.19	4.23±0.41
EW_{Fe}	eV	192.0±60.0	209.0±45.0	294.0±74.0	216.0±82.0
EM_1	10^{57} cm^{-3}	0.772±0.054	1.35±0.09	1.09±0.05	1.57±0.12
χ^2_ν		1.08	0.93	1.26	1.25
L_x	10^{33} ergs s^{-1}	51.40±2.60	50.20±2.68	46.50±2.18	43.31±3.91
$L_{x,unab}$	10^{33} ergs s^{-1}	69.59	69.42	61.59	60.50

[1]Dates given correspond to the midpoint of the observing interval

[2]TJD = JD - 2,450,000